Anal. Chem. **2005,** *77,* 735−741

Accelerated Articles

Direct Molecular Imaging of *Lymnaea stagnalis* Nervous Tissue at Subcellular Spatial Resolution by Mass Spectrometry

A. F. Maarten Altelaar,† Jan van Minnen,‡ Connie R. Jiménez,‡ Ron M. A. Heeren,† and Sander R. Piersma*,†

FOM—Institute for Atomic and Molecular Physics, Kruislaan 407, 1098 SJ Amsterdam, The Netherlands, and Department of Molecular and Cellular Neurobiology, Faculty of Earth and Life Sciences, Vrije Universiteit, De Boelelaan 1085, 1081 HV Amsterdam, The Netherlands

The imaging capabilities of time-of-flight secondary ion mass spectrometry (ToF−SIMS) and MALDI-MS sample preparation methods were combined. We used this method, named matrix-enhanced (ME) SIMS, for direct molecular imaging of nervous tissue at micrometer spatial resolution. Cryosections of the cerebral ganglia of the freshwater snail *Lymnaea stagnalis* were placed on indium−tin−oxide (ITO)-coated conductive glass slides and covered with a thin layer of 2,5-dihydroxybenzoic acid by electrospray deposition. High-resolution molecular ion maps of cholesterol and the neuropeptide APGWamide were constructed. APGWamide was predominantly localized in the cluster of neurons that regulate male copulation behavior of *Lymnaea*. ME-SIMS imaging allows direct molecule-specific imaging from tissue sections without labeling and opens a complementary mass window (<2500 Da) to MALDI imaging mass spectrometry at an order of magnitude higher spatial resolution (<3 μm).

Mapping the dynamic state of the proteome inside a specific cell or tissue section is a challenging area in biological research. Standard molecular tissue (imaging) analyses are usually performed by immunocytochemistry[1−3] or fluorescence microscopy.[4−7] In these affinity-based methods, a reporter molecule is linked to a target molecule using an antibody−antigen reaction, providing specific molecular information but limiting these techniques to known target molecules. Recently, imaging matrix-assisted laser desorption/ionization mass spectrometry (MALDI-MS) has been recognized as a tool for in situ proteomic analysis of (diseased) tissue.[8,9]

Imaging MS can spatially map surface components in tissue sections without pre-selection using the intrinsic property of molecular mass. The imaging MS approach for mapping protein and peptide distributions in mammalian tissues, developed in the group of Caprioli, has been seminal in the mass spectrometric community[10,11] and beyond.[12]

In imaging MS experiments, the ionization beam is rastered over the sample surface acquiring a data array of *x*,*y*-coordinates, with each position containing an entire mass spectrum. The current spatial resolution of MALDI microprobe imaging is in the 30−100-μm range,[13,14] although development of new instrumenta-

* Corresponding author. Telephone: +31-20-6081394. Fax: +31-20-6684106. E-mail: piersma@amolf.nl.

† FOM—Institute for Atomic and Molecular Physics.

‡ Vrije Universiteit.

(1) Croll, R. P.; van Minnen, J. *J. Comp. Neurol.* **1992**, *324*, 567−574.
(2) De Lange, R. P. J.; van Golen, F. A.; van Minnen, J. *Neuroscience* **1997**, *78*, 289−299.
(3) Horobin, R. W. *Biotech. Histochem.* **2002**, *77*, 3−13.
(4) Andersson-Engels, S.; Klinteberg, C.; Svanberg, K.; Svanberg, S. *Phys. Med. Biol.* **1997**, *42*, 815−824.
(5) Bastiaens, P. I. H.; Pepperkok, R. *Trends Biochem. Sci.* **2000**, *25*, 631−637.
(6) Wouters, F. S.; Verveer, P. J.; Bastiaens, P. I. H. *Trends Cell Biol.* **2001**, *11*, 203−211.
(7) Meyer, T.; Teruel, M. N. *Trends Cell Biol.* **2003**, *13*, 101−106.
(8) Aebersold, R.; Mann, M. *Nature* **2003**, *422*, 198−207.
(9) Hanash, S. *Nature* **2003**, *422*, 226−232.
(10) Caprioli, R. M.; Farmer, T. B.; Gile, J. *Anal. Chem.* **1997**, *69*, 4751−4760.
(11) Stoeckli, M.; Farmer, T. B.; Caprioli, R. M. *J. Am. Soc. Mass Spectrom.* **1999**, *10*, 67−71.
(12) Stoeckli, M.; Chaurand, P.; Hallahan, D. E.; Caprioli, R. M. *Nat. Med.* **2001**, *7*, 493−496.
(13) Chaurand, P.; Schwartz, S. A.; Caprioli, R. M. *Anal. Chem.* **2004**, *76*, 86a-93a.
(14) Kruse, R.; Sweedler, J. V. *J. Am. Soc. Mass Spectrom.* **2003**, *14*, 752−759.

10.1021/ac048329g CCC: $30.25
Published on Web 12/30/2004

tion with micrometer resolution has been reported.[15] With the current spatial resolution the technique is capable of mapping the molecular distribution at the tissue level but not at a cellular level, with most animal cells ranging from 5 to 50 μm in size.

Although secondary ion mass spectrometry (SIMS)[16] does not yield intact protein and peptide signals from cells and tissue sections, it does have several advantages as compared to MALDI. The most important advantage of SIMS over MALDI is the chemical imaging capabilities routinely delivering submicron spatial resolution.[17] Furthermore, the SIMS technique is very sensitive and remarkably versatile since it can analyze almost any kind of solid surface.[18] Using SIMS, imaging at subcellular spatial resolution of elements, in dynamic SIMS,[19−21] and small organic components, in static SIMS, has been achieved.[22−24] The difference between the two regimes is the density of the primary ion beam at the sample surface. In dynamic SIMS, a primary ion dose of approximately 10^{16} ions per cm^2 is used, which results in the sample surface being eroded in time and most molecular species being completely fragmented. In static SIMS, an ion dose $<10^{13}$ ions per cm^2 is used and only the first monolayer of the surface is damaged.[17,24,25] Consequently, the lower primary ion dose in static SIMS results in a higher ionization yield of intact, low molecular weight organic molecules as well as their fragments.

To enhance the desorption ("sputtering" in SIMS terminology) and ionization yield of intact molecular species in SIMS, fragmentation by the primary ion beam has to be minimized. MALDI is capable of producing ions at significantly higher masses than SIMS. In MALDI the matrix adsorbs most of the incident particle energy, thus preventing extensive fragmentation, which leads to soft ionization of the analyte molecules. Furthermore, fragmentation in the plume is reduced by collisional cooling with the matrix molecules.[26] MALDI sample preparation protocols combined with SIMS analysis have previously been shown to yield intact molecular ions for polymers, phospholipids, oligonucleotides and peptides, and proteins >10 kDa.[27−30] This technique is named matrix-enhanced (ME) SIMS. In ME-SIMS, standard MALDI matrixes are used, with 2,5-dihydroxybenzoic acid (DHB) giving signal intensity enhancement for the widest range of molecular species.[27] One of the advantages of ME-SIMS is that it is both easy and cheap to implement. Standard SIMS instrumentation and MALDI sample preparations protocols can be used.

When using MALDI sample preparation protocols in imaging MS, the most important parameter is optimal incorporation of the analyte into the matrix crystals with minimal lateral diffusion. Problems arise when the well-known dried droplet (DD) method[31] is used for matrix deposition. Matrix droplets deposited on top of a cryo-microtome cut tissue section with the DD method spread over the surface and crystallize. This leads to very large matrix crystal sizes (tens of microns) and lateral (*XY*) analyte diffusion after wetting of the surface. The resulting non-uniform matrix coverage of the sample surface severely hampers the spatial resolution of the technique. These problems can be overcome when the matrix arrives at the tissue surface in very small droplets, forming matrix crystals in the order of or smaller than the minimal lateral resolution of the imaging mass spectrometer used. Matrix solutions can be sprayed into small droplets using pneumatic nebulization (airbrush)[32] or electrospray deposition (ESD),[33,34] the latter method giving smaller and more monodisperse droplets.

Direct MALDI molecular profiling of biopsies, tissues, and whole cell extracts yield expression patterns, distributions, composition, and relative abundances of peptides and proteins.[35−39] The first successful direct MALDI analysis of neuropeptides from single cells was performed on *Lymnaea stagnalis* cells over a decade ago.[40,41] The freshwater snail *Lymnaea stagnalis* is a basommatophoran pulmonate, with a central nervous system containing only ~20 000 neurons that are clustered into a small number of major ganglia. Many of these neurons are peptidergic, of large size (50−150 μm), and easily identifiable from animal to animal.[42] Following the single-cell MALDI breakthrough, direct mass spectrometric analyses of invertebrate single neurons have provided a wealth of information about neuropeptides and their processing.[43,44] However, isolation of individual neurons is labori-

(15) Spengler, B.; Hubert, M. *J. Am. Soc. Mass Spectrom.* **2002**, *13*, 735−748.
(16) Vickerman, J. C.; Briggs, D. *ToF−SIMS*: *Surface Analysis by Mass Spectrometry*, 1st ed.; IM Publications and Surface Spectra Limited: Chichester, U.K., 2001.
(17) Todd, P. J.; McMahon, J. M.; Short, R. T.; McCandlish, C. A. *Anal. Chem.* **1997**, *69*, 529A−535A.
(18) Delcorte, A.; Garrison, B. J. *J. Phys. Chem. B* **2000**, *104*, 6785−6800.
(19) Chandra, S.; Morrison, G. H. *Int. J. Mass Spectrom.* **1995**, *143*, 161−176.
(20) Chandra, S.; Smith, D. R.; Morrison, G. H. *Anal. Chem.* **2000**, *72*, 104A−114A.
(21) Strick, R.; Strissel, P. L.; Gavrilov, K.; Levi-Setti, R. *J. Cell Biol.* **2001**, *155*, 899−910.
(22) Colliver, T. L.; Brummel, C. L.; Pacholski, M. L.; Swanek, F. D.; Ewing, A. G.; Winograd, N. *Anal. Chem.* **1997**, *69*, 2225−2231.
(23) Pacholski, M. L.; Cannon, D. M., Jr.; Ewing, A. G.; Winograd, N. *Rapid Commun. Mass Spectrom.* **1998**, *12*, 1232−1235.
(24) Todd, P. J.; Schaaff, T. G.; Chaurand, P.; Caprioli, R. M. *J. Mass Spectrom.* **2001**, *36*, 355−369.
(25) John, C. M.; Odom, R. W. *Int. J. Mass Spectrom.* **1997**, *161*, 47−67.
(26) Zenobi, R.; Knochenmuss, R. *Mass Spectrom. Rev.* **1998**, *17*, 337−366.
(27) Wu, K. J.; Odom, R. W. *Anal. Chem.* **1996**, *68*, 573−882.
(28) Hanton, S. D.; Cornelio Clark, P. A.; Owens, K. G. *J. Am. Soc. Mass Spectrom.* **1999**, *10*, 104−111.
(29) Wittmaack, K.; Szymczak, W.; Hoheisel, G.; Tuszynski, W. *J. Am. Soc. Mass Spectrom.* **2000**, *11*, 553−563.
(30) Luxembourg, S. L.; McDonnell, L. A.; Duursma, M. C.; Guo, X. H.; Heeren, R. M. A. *Anal. Chem.* **2003**, *75*, 2333−2341.
(31) Karas, M.; Hillenkamp, F. *Anal. Chem.* **1988**, *60*, 2299−2301.
(32) Schwartz, S. A.; Reyzer, M. L.; Caprioli, R. M. *J. Mass Spectrom.* **2003**, *38*, 699−708.
(33) Hensel, R. R.; King, R. C.; Owens, K. G. *Rapid Commun. Mass Spectrom.* **1997**, *11*, 1785−1793.
(34) Axelsson, J.; Hoberg, A. M.; Waterson, C.; Myatt, P.; Shield, G. L.; Varney, J.; Haddleton, D. M.; Derrick, P. J. *Rapid Commun. Mass Spectrom.* **1997**, *11*, 209−213.
(35) Li, L. J.; Garden, R. W.; Sweedler, J. V. *Trends Biotechnol.* **2000**, *18*, 151−160.
(36) Chaurand, P.; Caprioli, R. M. *Electrophoresis* **2002**, *23*, 3125−3135.
(37) Yanagisawa, K.; Shyr, Y.; Xu, B. G. J.; Massion, P. P.; Larsen, P. H.; White, B. C.; Roberts, J. R.; Edgerton, M.; Gonzalez, A.; Nadaf, S.; Moore, J. H.; Caprioli, R. M.; Carbone, D. P. *Lancet* **2003**, *362*, 433−439.
(38) Schwartz, S. A.; Weil, R. J.; Johnson, M. D.; Toms, S. A.; Caprioli, R. M. *Clin. Cancer Res.* **2004**, *10*, 981−987.
(39) Pierson, J.; Norris, J. L.; Aerni, H. R.; Svenningsson, P.; Caprioli, R. M.; Andren, P. E. *J. Proteome Res.* **2004**, *3*, 289−295.
(40) van Veelen, P. A.; Jimenez, C. R.; Li, K. W.; Wildering, W. C.; Geraerts, W. P. M.; Tjaden, U. R.; van der Greef, J. *Org. Mass Spectrom.* **1993**, *28*, 1542−1546.
(41) Jimenez, C. R.; van Veelen, P. A.; Li, K. W.; Wildering, W. C.; Geraerts, W. P. M.; Tjaden, U. R.; Vandergreef, J. *J. Neurochem.* **1994**, *62*, 404−407.
(42) Geraerts, W. P.; Smit, A. B.; Li, K. W.; Vreugdenhil, E.; van Heerikhuizen, H. In *Current Aspects of the Neurosciences*; Osborne, N. N., Ed.; McMillan Press: London, 1991; pp 255−305.
(43) Rubakhin, S. S.; Garden, R. W.; Fuller, R. R.; Sweedler, J. V. *Nat. Biotechnol.* **2000**, *18*, 172−175.
(44) Li, K. W.; Kingston, R.; Dreisewerd, K.; Jimenez, C. R.; van der Schors, R. C.; Bateman, R. H.; Geraerts, W. P. M. *Anal. Chem.* **1997**, *69*, 563−565.

ous, and only large, accessible neurons (such as the VD1 and the RPD2 neurons in *Lymnaea*[40,41,45]) can be sampled. In addition to mass spectrometric methods, neuropeptide distributions in nervous tissue of *L. stagnalis* have been characterized by means of molecular techniques[42] and immunocytochemistry.[1] Given the availability of both spatial as well as molecular information for *Lymnaea* neuropeptides, the brain of this mollusc represents an excellent model tissue for the development of high-resolution peptide imaging MS methodology. Mass spectrometric imaging at subcellular resolution can potentially map cell-specific neuropeptide distributions in tissue sections opening up a completely new analytical window.

EXPERIMENTAL SECTION

Materials. 2,5-Dihydroxybenzoic acid, trifluoracetic acid, and cholesterol were purchased from Sigma-Aldrich (Zwijndrecht, The Netherlands). HPLC-grade water and methanol were purchased from Merck (Darmstadt, Germany). APGWamide was synthesized as reported previously.[1]

Tissue Sampling Protocol. Freshwater snails (*L. stagnalis*) were raised under laboratory conditions; 20 ± 1 °C water temperature, 12 h light/12 h dark cycle, and fed lettuce ad libitum.[2] Adult specimens were decapitated, and the cerebral ganglia were dissected, directly embedded in 10% gelatine (De Twee Torens, Delft, The Netherlands) at 30 °C, and frozen at −80 °C. Gelatine embedding allows cryostat sectioning down to 5 μm thickness and does not interfere with ME-SIMS analysis. The 10-μm tissue sections were cut on a Leica CM 3000 cryostat (Leica Microsystems, Nussloch, Germany) at −20 °C. Sections were picked up on indium−tin−oxide (ITO, 4−8 Ω resistance) coated glass slides (Delta Technologies, Stillwater, MN), dried in a stream of warm air for 1 min, and then quickly frozen on dry ice and stored at −80 °C. Conservation of morphology was checked by optical microscopy during the sectioning, drying, and storage process. No obvious ice crystal damage was observed after freezing at −80 °C in gelatine. Light microscopy images were acquired using a Leica DMRX microscope with a Nikon DXM1200 digital camera. Prior to mass spectrometry, frozen tissue sections were brought to room temperature in a desiccator over a silica gel canister.

Extraction and Prepurification of Peptides. The commissure was dissected under a microscope and directly transferred to an eppendorf reaction tube. The peptides were extracted by adding 30 μL of 0.1 M acetic acid after which the solution was boiled for 5 min and sonicated for 5 min. The solution was centrifuged for 5 min at 14000 rpm, and the supernatant was purified using a C18 ZipTip column (Millipore corporation, Bedford, MA). For MS analysis, the extracts were spotted on a stainless steel target and diluted (1:1) with matrix solution (2,5-DHB in 50% aqueous acetonitrile).

Electrospray Matrix Deposition. For ESD, a syringe pump (KD Scientific, New Hope, PA) pumps matrix solution (15 mg/mL 2,5-DHB in 50% MeOH/0.1% TFA (V/V)) from a gastight syringe (Hamilton Bonaduz, Switzerland) through a stainless steel electrospray capillary (o.d. 220 μm, i.d. 100 μm) maintained at 3−5 kV. The capillary is mounted on an electrically isolated manual translation stage (Thorlabs, Newton, NJ) in a vertical orientation. The stage is fitted with a digital micrometer (Mitutoyo, Kawasaki, Japan) for accurate positioning of the needle tip with respect to the grounded sample plate. The sample plate is mounted on a X-Y moveable table (Thorlabs, Newton, NJ). Matrix deposition was performed by spraying for 10 min at a flow rate of 12 μL/h, a voltage of 4.7 kV, and a needle to sample plate distance of 5.0 mm.

Mass Spectrometry. All static SIMS experiments were performed on a Physical Electronics (Eden Prairie, MN) TRIFT-II time-of-flight SIMS (ToF−SIMS) equipped with an $^{115}In^+$ liquid metal ion gun, as described before.[46] In short, the TRIFT is a stigmatic imaging ToF analyzer incorporating a 2-m flight path and three quasi-hemispherical electrostatic sector analyzers (ESAs) as an integral part of the ToF analyzer. These ESAs compensate for the differences in ion flight times due to variations in the secondary ion's initial kinetic energies and ion emission angles. The secondary ions were extracted through a 3.2-kV electric field into the ToF analyzer and post-accelerated by an additional 5 kV prior to detection on a dual multichannel plate/phosphor screen detector. A multistop time-to-digital converter with 138-ps time resolution was used to acquire the detector signals.

All experiments were performed with a primary ion beam current of 450 pA, a primary pulse length of 30 ns, a spot diameter of 500 nm, and a primary ion energy of 15 kV. The experimental conditions were chosen in such a way that all the analyses were conducted in the static SIMS regime. For each chemical image, the primary beam was rastered over a 150 × 150 μm sample area, divided into 256 × 256 square pixels. The positive ion mode mass spectra and chemical images were taken from the same 150 × 150 μm areas within the sample. For each ion detected, the mass (ToF) and primary ion beam position were recorded, allowing post-processing of the data. The chemical images were compared to optical images of the corresponding sample areas.

MALDI ToF spectra were acquired using a Bruker BIFLEX (Bruker-Franzen Analytik, Bremen, Germany) system equipped with a SCOUT ion source and a 337-nm nitrogen laser VSL-337i (Laser Science, Newton, MA). All analyses shown here were carried out in the reflectron mode with an acceleration voltage of 20 kV.

Scanning Electron Microscopy. Measurements were performed on a FEI XL30 SFEG scanning electron microscope (SEM) (FEI company, Eindhoven, The Netherlands). The accelerator voltage of the system was 2−3 kV. Samples were coated with a thin carbon layer to improve the conductivity of the sample and so prevent charge accumulation.

RESULTS AND DISCUSSION

Figure 1 compares the spectra of a commissure extract of nervous tissue of *L. stagnalis* obtained using (A) ME-SIMS with a 15-kV ^{115}In primary ion beam and (B) MALDI-MS using a 337-nm nitrogen laser. In both experiments, standard DD sample preparation protocols were used with 2,5-DHB as matrix. The spectra are highly similar in the mass range up to 2500 Da. Peptides present in the commissure are mainly derived from the caudodorsal cell hormone (CDCH) precursor, which initiates egg

(45) Jimenez, C. R.; Li, K. W.; Dreisewerd, K.; Spijker, S.; Kingston, R.; Bateman, R. H.; Burlingame, A. L.; Smit, A. B.; van Minnen, J.; Geraerts, W. P. M. *Biochemistry* **1998**, *37*, 2070−2076.

(46) Schueler, B. W. *Microsc. Microanal.* **1992**, *3*, 119−139.

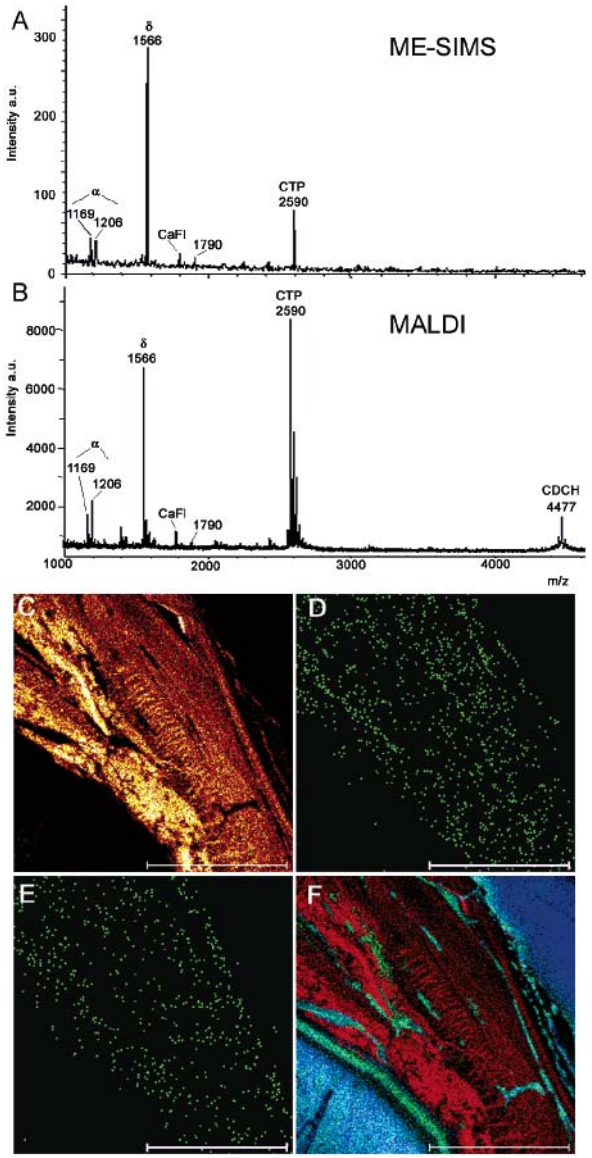

Figure 1. ME-SIMS vs MALDI. (A) ME-SIMS and (B) MALDI spectrum of a commissure extract of the pond snail *Lymnaea stagnalis*. Both spectra were obtained using standard dried droplet sample preparation with 2,5-DHB as matrix. The peptides identified are α-caudorsal cell peptide (α, protonated and cationized), δ peptide (δ), HFFYGPYDVFQRDVamide (*m*/*z* 1790), Calfluxin (CaFl), carboxyl terminal peptide (CTP), and caudodorsal cell hormone (CDCH). The ME-SIMS measurements used indium primary ions (total ion dose 8.9×10^{11} ions/cm^2) and the MALDI experiments 250 shots of the 4-ns 337-nm nitrogen laser. (C−F) SIMS images of dried droplet sample preparation, with (C) 2,5-DHB (154 *m*/*z*, 0−14 counts), (D) δ-peptide (1566 *m*/*z*, 0−2 counts), (E) CTP-peptide (2590 *m*/*z*, 0−2 counts), and (F) overlay of 2,5-DHB (red, 0−14 counts), sodium (blue, 0−5 counts), and potassium (green, 0−10 counts). Scale bars are 100 μm.

laying in *Lymnaea*.[47] Peptides derived from the CDCH precursor and present in both spectra are as follows: αCDCP (protonated and cationized), δ peptide, Calfluxin (CaFl), and the carboxyl terminal peptide (CTP). In addition, the recently described HFFYGPYDVFQRDVamide (*m*/*z* 1790),[47] not encoded by the CDCH precursor, was detected as well. In the MALDI spectrum an additional mass can be seen at 4477 *m*/*z*, corresponding to the protonated CDCH precursor, not observed in the ME-SIMS spectrum. There are two principal factors why the higher mass peptide is not seen in the ME-SIMS spectrum. First, the desorption and ionization process of both techniques differ significantly, as explained elsewhere.[48] Second, given the lower mass range of conventional SIMS, the TRIFT has been optimized for low mass ions (< *m*/*z* 2500). The limited post-acceleration (8 kV) results in reduced detection efficiency for larger molecules[49] like the peptide at 4477 *m*/*z*. The ME-SIMS peptide analysis of a biological extract exemplifies the use of SIMS together with standard MALDI sample preparation protocols in the analysis of peptides with a molecular weight up to 2500 Da, at biologically relevant concentrations. Omitting the matrix yielded SIMS spectra with signals only ranging up to 200 Da and did not show any molecular signals.

The imaging capabilities of the SIMS instrument allowed spatial analysis of the molecular distribution of the matrix and peptide molecules in the DD experiment, as shown in Figure 1, panels C−F. The matrix signal in Figure 1C shows a single crystal >150 μm in length and ~100 μm in width, formed using the DD method. The peptide signals (Figure 1D,E) are confined to the matrix crystals, while the cations are segregated (Figure 1F) as observed earlier.[30] These large matrix crystals are not an issue in MALDI imaging studies where the laser spot-size ranges between 20 and 50 μm.[13,14] Since the typical SIMS experimental spatial resolution is 1 μm,[17] these large crystals will interfere with the SIMS spatial analysis. So, in order not to compromise the obtainable spatial resolution in ME-SIMS, the matrix crystals must be 1 μm or smaller. Electrospray matrix deposition results in the required matrix crystal sizes (≤ 1 μm).

For the direct molecular imaging of *L. stagnalis* nervous tissue by ME-SIMS, 10 μm thick tissue sections were cut using a cryomicrotome. The tissue sections were covered with 2,5-DHB as moderating matrix. Figure 2A shows an optical image of a tissue section of the central nervous system of *Lymnaea*; labeled regions are the left and right cerebral ganglia (Cg_l and Cg_r), connecting commissure (Cm), dorsal bodies (Db), and left and right anterior lobe (Al_l and AL_r). In the inset of Figure 2A, a high magnification image of the anterior lobe is presented (boxed area), clearly showing the large neurons and their nuclei, indicated by the red arrows. Approximately 120−150 neurons are present in the right anterior lobe, playing a central role in the reproduction of *Lymnaea*.[1,2,50]

ME-SIMS spectra of *Lymnaea* nervous tissue, after ESD, show cholesterol signals at 386 *m*/*z* $(M)^+$ and the dominant fragment ion at 369 *m*/*z* $(M\text{-}OH)^+$, a signal at 430 *m*/*z*, and lower abundance masses in the range of 500−1000 *m*/*z* (Figure 3). The 430 *m*/*z* signal is assigned to the neuropeptide APGWamide, previously structurally characterized by single-cell MALDI MS/MS[44] and localized by immunocytochemistry.[1] APGWamide plays a key role in the regulation of the male reproductive activity of *Lymnaea*.

(47) Jimenez, C. R.; ter Maat, A.; Pieneman, A.; Burlingame, A. L.; Smit, A. B.; Li, K. W. *J. Neurochem.* **2004**, *89*, 865−875.

(48) McDonnell, L. A.; Piersma, S. R.; Altelaar, A. F. M.; Mize, T. H.; Luxembourg, S. L.; Verhaert, P.; Minnen van, J.; Heeren, R. M. A. *J. Mass Spectrom.* (in press).

(49) Gilmore, I. S.; Seah, M. P. *Int. J. Mass Spectrom.* **2000**, *202*, 217−229.

(50) De Lange, R. P. J.; van Minnen, J. *Gen. Comp. Endocrinol.* **1998**, *109*, 166−174.

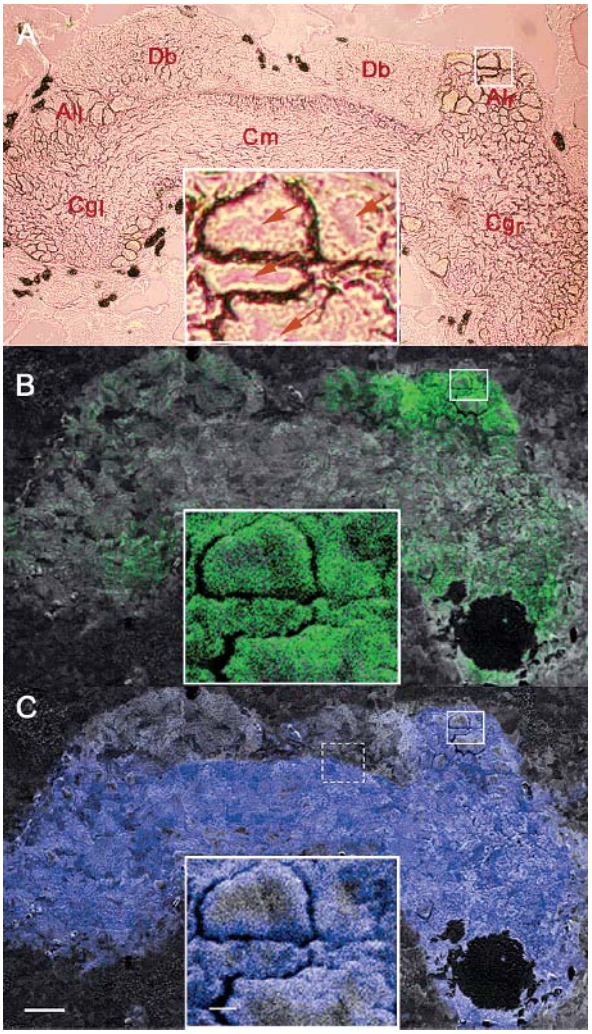

Figure 2. Direct molecular imaging of *Lymnaea stagnalis* nervous tissue by ME-SIMS. (A) Optical image of the *Lymnaea* cerebral ganglia, inset shows high magnification image of neurons in the anterior lobe (solid box), arrows indicate nuclei. Different regions in the section are right and left cerebral ganglia (Cg_r and Cg_l), anterior lobe (Al), commissure (Cm), and dorsal bodies (Db). (B) ME-SIMS image of APGWamide (429.0−433.2 *m*/*z*; green, 0−3 counts) distribution. (C) ME-SIMS image of cholesterol (368.2−371.3 *m*/*z*; blue, 0−4 counts) distribution. Scale bar: 200 μm; scale bar inset: 10 μm. Molecular images (B and C) are presented as colored overlays on top of the gray-scale TIC (total ion count) image (mass range: 1.0−5000 *m*/*z*, 0−140 counts). The ME-SIMS measurements used indium primary ions (total ion dose 4.9×10^{11} ions/cm^2).

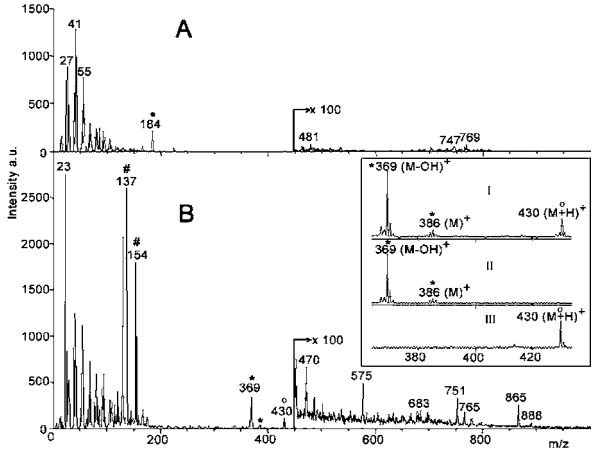

Figure 3. ToF−SIMS spectra of the *Lymnaea* nervous tissue before (A) and after (B) ESD matrix deposition. Marked peaks are 2,5-DHB $(M)^+$ at 154 *m*/*z* and $(M - OH)^+$ at 137 *m*/*z* (#), phosphocholine fragment ion at 184 *m*/*z* (●), cholesterol $(M)^+$ at 386 *m*/*z* and $(M - OH)^+$ at 369 *m*/*z* (*), and APGWamide $(M + H)^+$ at 430 *m*/*z* (○). Inset shows (I) zoomed area of spectrum B and ME-SIMS spectra of (II) synthetic cholesterol and (III) synthetic APGWamide.

cDNA studies have shown that from every precursor protein 10 copies of APGWamide are synthesized, together with single copies of several other peptides.[44,50,51] In addition to the low *m*/*z* ions (<130 *m*/*z*) and the matrix ions (154 and 137 *m*/*z*), the cholesterol and the APGWamide signal were intense enough for ME-SIMS imaging.

The sampled area in one ToF−SIMS experiment was 150 × 150 μm. To image a larger section, the sample stage was stepped in a mosaic pattern, and the resulting images were aligned to produce a single molecular image. To cover the entire tissue section, 77 SIMS experiments of 3 min per experiment were conducted. In Figure 2B,C, mass spectral images of the same tissue section as in Figure 2A are shown after matrix deposition, ME-SIMS data acquisition, and processing. The total ion count (TIC) images are presented in gray-scale and overlaid with the molecular images of APGWamide (green) and cholesterol (blue). ME-SIMS images of *Lymnaea* nervous tissue show that APGWamide is predominantly localized in the right anterior lobe (Figure 2B). In addition to the strong APGWamide signal in the right anterior lobe, less abundant localization can be found in the left anterior lobe and in the left and right cerebral ganglion, which is in agreement with immunocytochemistry results.[1] Nonhomogeneous subcellular APGWamide distributions were observed for the large neurons in the anterior lobe (Figure 2B inset). The higher cytosolic neuropeptide signals contrast with the central darker part of the cell corresponding to the nucleus. Indeed precursor and active peptides are packaged in cytosolically localized, secretory vesicles,[52] in line with the ME-SIMS data.

Cholesterol signals are found in comparable intensity on the entire tissue section except for the dorsal bodies, non-nervous neuroendocrine organs located at the dorsal surface of the cerebral ganglia,[53] where signal intensity is decreased (Figure 2C). The origin for the difference in cholesterol signal intensity in the ME-SIMS image is unclear. In the optical image (Figure 2A), it can be seen that the tissue morphology of the dorsal bodies differs from the rest of the section. The highest cholesterol signal is obtained at the cellular plasma membrane but not at the nuclear membrane (Figure 2C inset), in line with recent observations on cholesterol localization.[54−57] These results illustrate the subcellular imaging capabilities of the ME-SIMS technique. In the TIC image

(51) Smit, A.; Jimenez, C.; Dirks, R.; Croll, R.; Geraerts, W. *J. Neurosci.* **1992**, *12*, 1709−1715.
(52) Hook, V.; Azaryan, A.; Hwang, S.; Tezapsidis, N. *FASEB J.* **1994**, *8*, 1269−1278.
(53) Joosse, J. *Arch. Ned. Zool.* **1964**, *16*, 1−103.
(54) Liscum, L.; Munn, N. J. *Mol. Cell Biol.* **1999**, *1438*, 19−37.
(55) Rukmini, R.; Rawat, S. S.; Biswas, S. C.; Chattopadhyay, A. *Biophys. J.* **2001**, *81*, 2122−2134.
(56) Simons, K.; Ikonen, E. *Science* **2000**, *290*, 1721−1726.
(57) Sjovall, P.; Lausmaa, J.; Nygren, H.; Carlsson, L.; Malmberg, P. *Anal. Chem.* **2003**, *75*, 3429−3434.

the cellular outlines can be observed readily, especially for large neurons (see insets Figure 2). The TIC image contains in each pixel the sum of all ions (elements, low-mass-fragment ions, and molecular ions) arriving at the detector for a given location on the tissue. Although molecular information is not obtained in the TIC images, morphological detail is comparable with conventional light microscopy, allowing the alignment of 77 individual images of 150 × 150 μm into a mosaic pattern. The overlay of TIC and molecular images thus combines both morphological and molecular information.

Cholesterol and APGWamide ME-SIMS signals are confined to the tissue section. This indicates that neither the tissue-sampling protocol nor the electrospray matrix deposition method give rise to extensive peptide redistribution over the surface at the micrometer scale, corroborating the observations of Kruse et al.[14] The images in Figure 2B,C show a circular hole in the lower right cerebral ganglion where, due to an electrospray artifact, no matrix was deposited. The clear boundary of the circular hole shows that migration of analyte-doped matrix crystals on top of a tissue section does not occur. Furthermore, in the absence of matrix (the hole), the molecular ion signals, seen in the area with matrix, were absent. ToF−SIMS imaging experiments of *Lymnaea* nervous tissue sections without the application of a moderating matrix gave very few high mass signals except for m/z 184 (Figure 3A). The signal at m/z 184 is attributed to phosphocholine, the polar headgroup of the lipids phosphatidylcholine (PC) and sphingomyelin (SM),[58,59] the two major constituents of the lipid bilayer in the brain. This result is in agreement with earlier SIMS studies, where the phosphocholine headgroup was used for imaging of the PC distribution.[17,60,61]

Matrix addition does complicate the SIMS imaging analysis since it modifies the tissue surface. A comparison of the DD and the ESD methods by SIMS revealed a highly nonuniform distribution of the matrix over the surface in the DD sample. Furthermore, the sample consisted of regions with abundant peptide signal next to regions where no peptide signal was detected, although matrix molecules were present. The SIMS images obtained after ESD, however, showed a uniform distribution of the same selected ions. These results are in agreement with previous studies where it has been shown that in the DD method highly nonuniform matrix crystals are formed.[28,30,62] These local matrix crystal variations will result in unrepresentative images of the molecular distribution in a tissue, when using the DD method in combination with the high spatial resolution of imaging ToF−SIMS. Figure 4 shows scanning electron microscopy (SEM) images of the surface of *Lymnaea* nervous tissue before (Figure 4A) and after (Figure 4B,C) ESD. The SEM images clearly show that homogeneously distributed, submicron-sized (length ~0.5−1 μm, width ~0.2−0.4 μm) crystals are formed (Figure 4C). For comparison, the heterogeneously distributed matrix crystals formed on-tissue from the dried droplet method appeared in sizes exceeding 20 μm (data not shown).

The resolving power of molecular imaging of biological tissues by ME-SIMS is a convolution of the SIMS instrument spatial resolution (primary ion beam focus) and the tissue sampling/matrix deposition protocol. To determine the resolving power of the ME-SIMS imaging method, the sharp decrease in cholesterol (m/z 369) signal intensity going from the commissure to the dorsal bodies is examined. A (30-μm) line scan was taken (Figure 5), and the resolving power was defined by taking the length Δx required to go from 80% to 20% cholesterol signal intensity.[22] Cholesterol intensity data (●) along the line were fitted with a

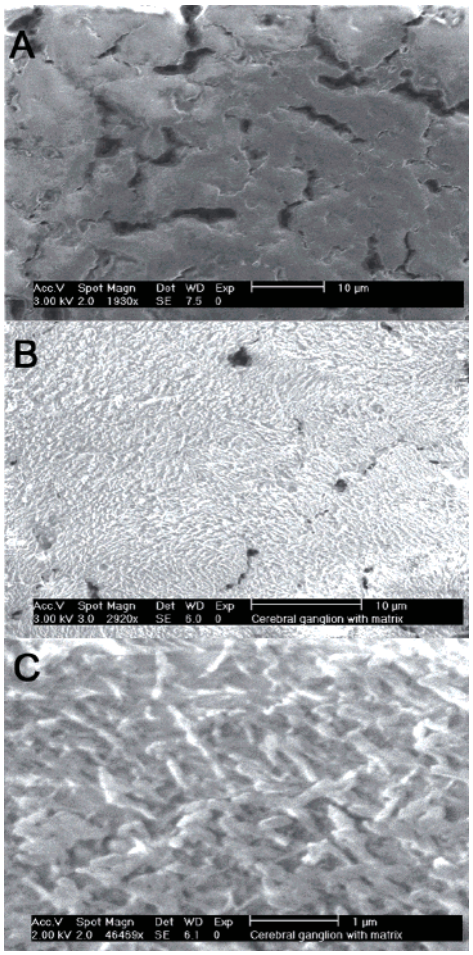

Figure 4. Scanning electron microscopy images of *Lymnaea stagnalis* nervous tissue (A) prior to matrix application (scale bar 10 μm) and (B) after ESD of 2,5-DHB (scale bar 10 μm). (C) Higher magnification image showing submicron crystal dimensions after ESD (length ~0.5−1 μm, width ~0.2−0.4 μm) (scale bar 1 μm).

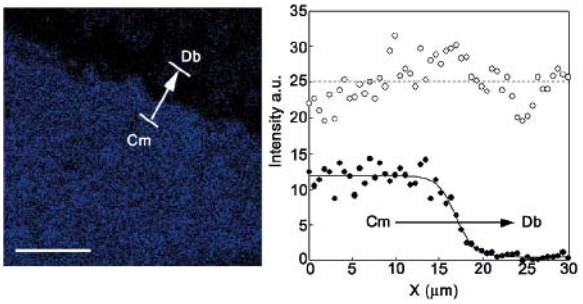

Figure 5. Experimental resolution of direct tissue ME-SIMS. (A) Cholesterol distribution (blue) in the commissure (Cm) and dorsal body (Db) area (dashed box in Figure 2C). Scale bar: 50 μm. The arrow indicates a line scan orthogonal to the commissure−dorsal body transition (length 30 μm, width 3.5 μm). (B) Cholesterol (●) and 2,5-DHB intensity data (○) of the same line scan.

(58) Hsu, F. F.; Turk, J. *J. Am. Soc. Mass Spectrom.* **2000**, *11*, 437−449.
(59) Hsu, F. F.; Turk, J. *J. Am. Soc. Mass Spectrom.* **2003**, *14*, 352−363.
(60) McMahon, J. M.; Short, R. T.; McCandlish, C. A.; Brenna, J. T.; Todd, P. J. *Rapid Commun. Mass Spectrom.* **1996**, *10*, 335−340.
(61) Ostrowski, S. G.; Van Bell, C. T.; Winograd, N.; Ewing, A. G. *Science* **2004**, *305*, 71−73.
(62) Garden, R. W.; Sweedler, J. V. *Anal. Chem.* **2000**, *72*, 30−36.

sigmoidal function $I = I_0 + a/[1 + e^{(x-x_0/b)}]$ (solid line) defining the length Δx. Fitted values are as follows: $I_0 = 0.56 \pm 0.28$ counts, $a = 11.41 \pm 0.37$ counts, $b = -1.06 \pm 0.19$ μm, and $x_0 = 16.90 \pm 0.22$ μm with $R = 0.979$. A lateral resolving power (Δx) of 2.9 μm was calculated (with $I - I_0 = 100\%$). For comparison, the 2,5-DHB signal (○) along the same line scan showed homogeneous coating of the tissue section surface by the matrix. If extensive analyte diffusion/redistribution would occur due to cryostat sectioning, drying, or surface wetting during ESD, then this should result in decreased resolution. The calculated resolving power of 2.9 μm, a factor ~3 lower than the SIMS experimental resolution (1 μm), indicates that the tissue sampling and matrix deposition protocol does not excessively compromise the spatial resolution in ME-SIMS.

Alternative matrixes have been used in SIMS to enhance the sensitivity of high molecular weight molecules. Sjövall et al. made imprints of biological samples on a silver surface,[57] and Nygren et al. used a thin layer of sputtered silver on top of cells[63] and tissue.[64] The use of silver as matrix allowed high-resolution imaging of the cholesterol ion distribution in cells and tissue. More recently, SIMS papers have appeared where the use of polyatomic primary ion sources is discussed.[65−69] The great benefit of the use of these primary ion beams is the enhancement of the secondary ion emission of relatively large molecules. Touboul et al.[67] showed intense molecular ion signals for a synthetic phospholipid and peptides in the presence of nitrocellulose, using a Au_3^+ cluster ion beam. A matrix (nitrocellulose) was still needed to obtain the molecular ion signal, while in a cellular extract phospholipid signals could be obtained without nitrocellulose.[67] SIMS imaging studies of mouse brain tissue sections using a Au_3^+ cluster ion beam revealed the spatial distribution of cholesterol and several lipids.[67,68] A direct comparison of the resolving power with Au_3^+ cluster ion beams and ME-SIMS is difficult since the authors used a different definition (pixel size) for the spatial resolution. However, inspecting the molecular images and signal intensity profiles in the study of Sjövall et al.[68] (Figures 3 and 4), we estimate the resolving power with the Au_3^+ cluster ion beam in direct tissue analysis to be in the order of 5−10 μm, 2−3-fold higher than in ME-SIMS imaging.

MALDI imaging has been used to investigate neuropeptide distributions in single neurons.[70] The low spatial resolution (50 μm pixel size) did not allow for subcellular localization of these peptides in relatively large neuronal cells (100 μm). MALDI imaging in microprobe mode is very well suited for spatially profiling of high mass molecules at the tissue level,[13,14] but currently, the maximum obtainable spatial resolution is insufficient for (sub)cellular imaging. Chemical imaging MS using an ion-optical microscope[71] eliminates the need for a tightly focused ionization beam. Here the spatial resolution is determined by the ion optics of the mass spectrometer. This stigmatic ion imaging mass spectrometer permits the use of ionization beams that are difficult to focus, such as UV and IR laser beams or C_{60} polyatomic primary ion beams, in high-resolution imaging of (biological) surfaces. Luxembourg et al.[71] have recently demonstrated the capability of this ion-optical microscope to map the distribution of ions as large as insulin (m/z 5733) using an UV MALDI ionization beam, with an overall spatial resolution of 4 μm.

CONCLUSIONS

We have shown that direct molecular imaging of nervous tissue at subcellular resolution is feasible by using matrix-enhanced SIMS. Electrospray matrix deposition preserves the spatial distribution of surface analytes in tissue sections and allows peptide ionization using SIMS.

ME-SIMS localized the peptide APGWamide in the anterior lobe of the right Cg, consistent with immunocytochemical data. The spatial resolution of peptide imaging by ME-SIMS is about 1 order of magnitude better than that of microprobe mode imaging MALDI.

ACKNOWLEDGMENT

The authors thank Jaap J. Boon, Liam A. McDonnell, and Ka-Wan Li for stimulating discussions and Ilya Cerjak and Hildo Vader for the design and construction of the electrospray setup. This work is part of the Research Program 49 “Mass Spectrometric Imaging and Structural Analysis of Biomacromolecules” of the “Stichting voor Fundamenteel Onderzoek der Materie (FOM)”, which is financially supported by the ”Nederlandse Organisatie voor Wetenschappelijk Onderzoek (NWO)”.

Received for review November 12, 2004. Accepted December 14, 2004.

AC048329G

(63) Nygren, H.; Malmberg, P. *J. Microsc.* (*Oxford*) **2004**, *215*, 156−161.
(64) Nygren, H.; Malmberg, P.; Kriegeskotte, C.; Arlinghaus, H. F. *FEBS Lett.* **2004**, *566*, 291−293.
(65) Townes, J. A.; White, A. K.; Wiggins, E. N.; Krantzman, K. D.; Garrison, B. J.; Winograd, N. *J. Phys. Chem. A* **1999**, *103*, 4587−4589.
(66) Nguyen, T. C.; Ward, D. W.; Townes, J. A.; White, A. K.; Krantzman, K. D.; Garrison, B. J. *J. Phys. Chem. B* **2000**, *104*, 8221−8228.
(67) Touboul, D.; Halgand, F.; Brunelle, A.; Kersting, R.; Tallarek, E.; Hagenhoff, B.; Laprevote, O. *Anal. Chem.* **2004**, *76*, 1550−1559.
(68) Sjovall, P.; Lausmaa, J.; Johansson, B. *Anal. Chem.* **2004**, *76*, 4271−4278.
(69) Weibel, D. E.; Lockyer, N.; Vickerman, J. C. *Appl. Surf. Sci.* **2004**, *231−232*, 146−152.
(70) Rubakhin, S. S.; Greenough, W. T.; Sweedler, J. V. *Anal. Chem.* **2003**, *75*, 5374−5380.
(71) Luxembourg, S. L.; Mize, T. H.; McDonnell, L. A.; Heeren, R. M. A. *Anal. Chem.* **2004**, *76*, 5339−5344.